PROCEEDINGS OF SPIE

SPIEDigitalLibrary.org/conference-proceedings-of-spie

A four mirror anastigmat collimator design for optical payload calibration

Stephen Rolt, Ariadna Calcines, Bart Lomanowski, David Bramall

Stephen Rolt, Ariadna Calcines, Bart A. Lomanowski, David G. Bramall, "A four mirror anastigmat collimator design for optical payload calibration," Proc. SPIE 9904, Space Telescopes and Instrumentation 2016: Optical, Infrared, and Millimeter Wave, 99044U (29 July 2016); doi: 10.1117/12.2232327

Event: SPIE Astronomical Telescopes + Instrumentation, 2016, Edinburgh, United Kingdom

A Four Mirror Anastigmat Collimator Design for Optical Payload Calibration

Stephen Rolt, Ariadna Calcines, Bartosz A. Lomanowski and David G. Bramall

Centre for Advanced Instrumentation, Univ. of Durham, William Armstrong Way, Sedgefield, Co. Durham, United Kingdom, TS21 3FH.

ABSTRACT

We present here a four mirror anastigmatic optical collimator design intended for the calibration of an earth observation satellite instrument. Specifically, the collimator is to be applied to the ground based calibration of the Sentinel-4/UVN instrument. This imaging spectrometer instrument itself is expected to be deployed in 2019 in a geostationary orbit and will make spatially resolved spectroscopic measurements of atmospheric contaminants.

The collimator is to be deployed during the ground based calibration only and does not form part of the instrument itself. The purpose of the collimator is to provide collimated light within the two instrument passbands in the UV-VIS (305 – 500 nm) and the NIR (750 – 775 nm). Moreover, that collimated light will be derived from a variety of slit like objects located at the input focal (object) plane of the collimator which is uniformly illuminated by a number of light sources. The collimator must relay these objects with exceptionally high fidelity. To this end, the wavefront error of the collimator should be less than 30 nm rms across the collimator field of view. This field is determined by the largest object which is a large rectangular slit, 4.4° x 0.25°. Other important considerations affecting the optical design are the requirements for input telecentricity and the size (85 mm) and location (2500 mm 'back focal distance') of the exit pupil.

The design of the instrument against these basic requirements is discussed in detail. In addition an analysis of the straylight and tolerancing is presented in detail.

Keywords: Collimator, anastigmat, form error, straylight, tolerance modelling, off-axis conic

1. INTRODUCTION

1.1 Background

The purpose of the collimator is to provide uniform illumination of the Sentinel-4 /UVN instrument slit by evenly irradiating the instrument input pupil. The S4-UVN instrument is an imaging spectrometer whose ultimate purpose is to image the spectral irradiance of the Earth with a view to spectroscopically mapping atmospheric contaminants[1,2]. It is to operate across two distinct spectral bands, the UV-VIS (305-500 nm) and the NIR (750 – 775 nm). During the ground based test programme, the instrument, which is to be located in a thermal vacuum chamber during tests, focusses the collimated beam onto its slit before passage through the remainder of the spectrometer.

Located at the focal plane of the collimator are a number of object targets which are uniformly illuminated by a variety of continuum and monochromatic sources. These object target most generally take the form of slit like or point objects

Space Telescopes and Instrumentation 2016: Optical, Infrared, and Millimeter Wave, edited by Howard A. MacEwen, Giovanni G. Fazio, Makenzie Lystrup, Proc. of SPIE Vol. 9904, 99044U · © 2016 SPIE · CCC code: 0277-786X/16/$18 · doi: 10.1117/12.2232327

which must be faithfully reproduced by the collimator optics. Figure 1 provides a schematic illustration of the test set up.

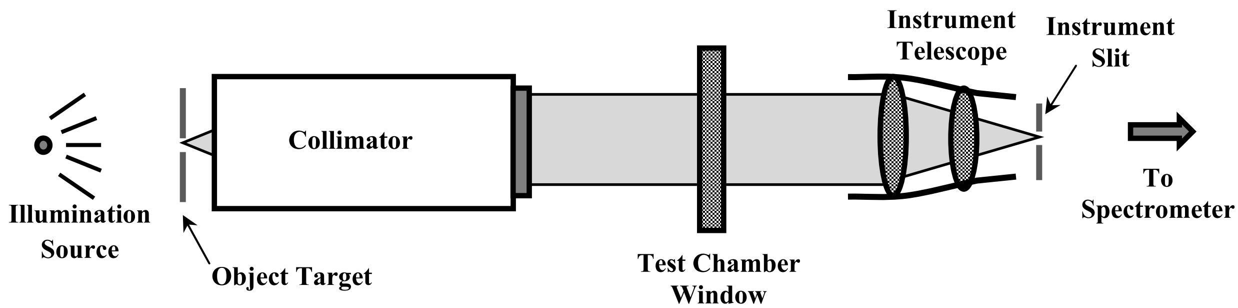

Figure 1: General optical arrangement showing collimator deployed during testing of the S4 UVN Instrument.

Of course, in this article, only the performance of the collimator alone is of interest. Faithful replication of sharp object features by the collimator is an essential requirement of the overall instrument calibration process. A variety of objects are to be deployed at the object target location. These include, as suggested, a number of linear/rectangular features and a line of point sources (pinholes). The overall extent of the object field amounts to 4.2° x 0.5°. Accurate replication of these features by the collimator is articulated by a wavefront error requirement for the collimator of 30 nm RMS across the wavelength range and all fields. In addition to direct calibration of the spectrometer and slit function and detector sensitivity etc., great emphasis is also placed upon the removal of background light in any measurements. Therefore, the straylight contribution of the collimator unit must be restricted as far as possible. Finally, the first order parameters of the collimator are defined by requirements for the output pupil size (80-90 mm) and location (2500 mm from the collimator) and the requirement for telecentricity.

1.2 Collimator Design Considerations

The most salient design requirement is the ambitious wavefront error target of 30 nm RMS across the entire spectral range from 305-775 nm. This requirement includes defocus and, as such, any chromatic effects will contribute to the total. With this in mind, therefore, the design must be substantially achromatic. As a consequence of the wide spectral range and ambitious target, the use of transmissive optics is precluded. Therefore, the design must be restricted to an all mirror design.

With a mirror design, only correction of the classical monochromatic aberrations is necessary. The only relevant first order design constraint, apart from the size of the field, is the output pupil size and location. Thus there is freedom, within reason, to select the system numerical aperture. In this instance, a system aperture of f#10 is selected, giving an effective focal length of 850 mm for an 85 mm pupil. In principle, to reduce aberrations, the system needs to be as ‘slow’ as possible. This consideration is, in practice, constrained by the need to make the system reasonably compact and f#10 represents a reasonable compromise.

Due to the relatively modest aperture and field angle range, only correction of the five primary Gauss-Seidel aberrations is necessary. Correction of these aberrations would, at first sight, require the use of three mirrors. This, of course, forms the basis of the well-known Three Mirror Anastigmat (TMA) design[3,4]. However, in this specific case, an additional constraint is imposed – that of telecentricity. Therefore, in this design, an additional mirror is introduced to provide an extra degree of freedom and the four design constraints on mirror curvature may be listed, as below:

i) Position of collimator focus
ii) Collimator focal length
iii) Zero Petzval sum
iv) Pupil focus at infinite conjugate

As with the TMA, this four mirror anastigmat design uses conics. In this case, the conics are off-axis.

2: DESCRIPTION OF DESIGN

2.1 Object Targets

This paper considers the design of the collimator itself. Details of the illumination system are not covered. However a brief description of the object targets will be given. These are moveable targets, that is to say, different object patterns can be inserted into the object field by movement of a mask pattern. This is illustrated in Figure 2.

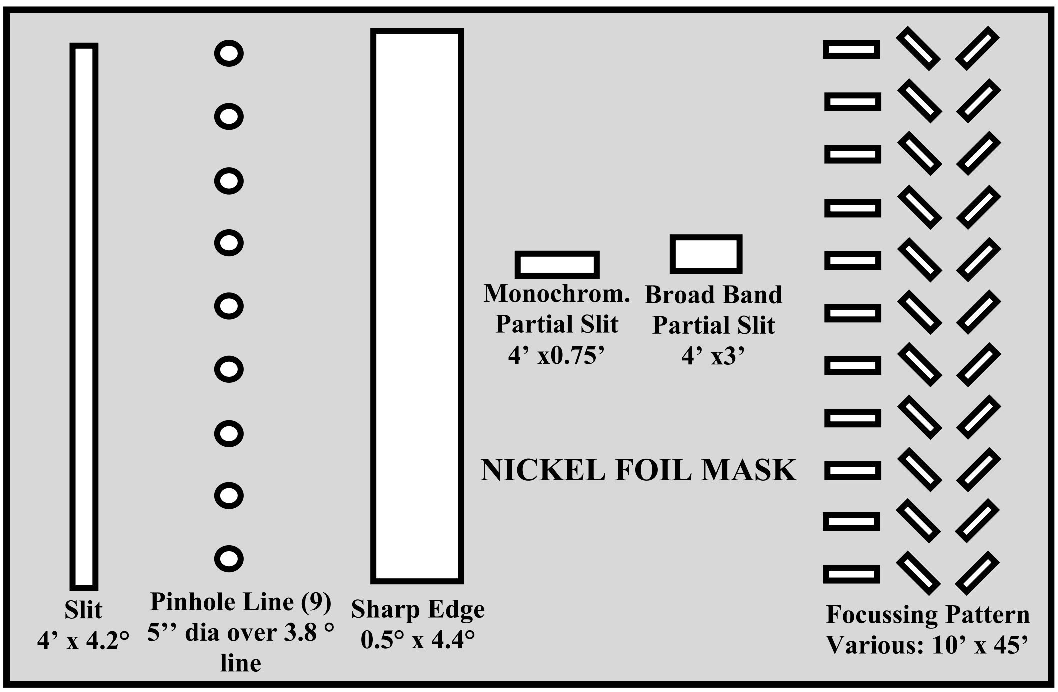

Figure 2: Object targets. These objects consist of a nickel foil with apertures mounted on a ceramic plate.

With an effective focal length of 850 mm, the sharp edge target, for example, consists of an aperture 70 x 8 mm. At any one time, only one of the patterns illustrated in Figure 2 will be deployed. Selection will be by lateral translation of the mask. The patterns are to be illuminated by one of four illumination sources:

i) Continuum (Xenon arc) source
ii) Filter light source (Xenon arc lamp + narrowband filter)
iii) Monochromatic light source (spectral lamp for wavelength calibration)
iv) Tunable source (tunable narrowband laser system)

2.2 Main Collimator Design

A simplified layout of the collimator design is shown in Figure 3. Any obscuration of the collimator is not permitted and, therefore, the design must be an off-axis design. Most importantly, to minimise aberrations, the sense of the off-axis tilts is across the line of the slit where the field angles are much smaller (0.5° vs. 4.4°). The design was optimised using ray tracing software and employing a merit function based on wavefront error across the object field.

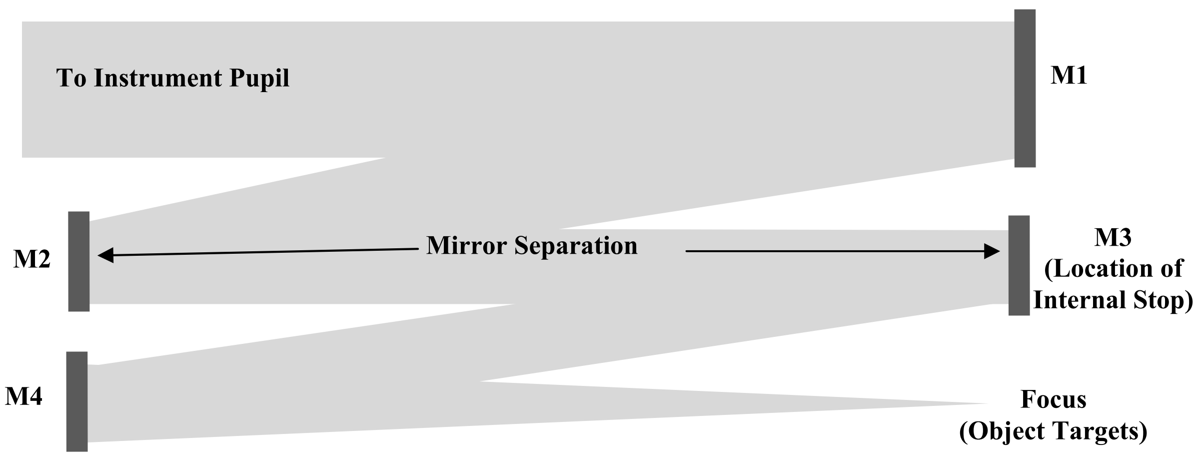

Figure 3 Simplified Layout of Collimator. This shows the four main mirrors – an additional fold mirror is not shown here.

All mirrors, with the exception of the second mirror, M2, are off-axis conics. The choice of off-axis conics, as opposed to off-axis aspheres provides design flexibility but without adding to manufacturing complexity. Off-axis aspheres are difficult to manufacture and particularly difficult to test. The second mirror, which lies close to an intermediate focal plane, is a sphere. The internal collimator stop is located close to the third mirror and is imaged, as required, 2500 mm from the collimator. Separation of the two groups of mirrors amounts to about 900 mm. Not shown in Figure 3 is an additional fold mirror located close to the object target. The system is shown in a little more detail in the modelled ray trace set out in Figure 4.

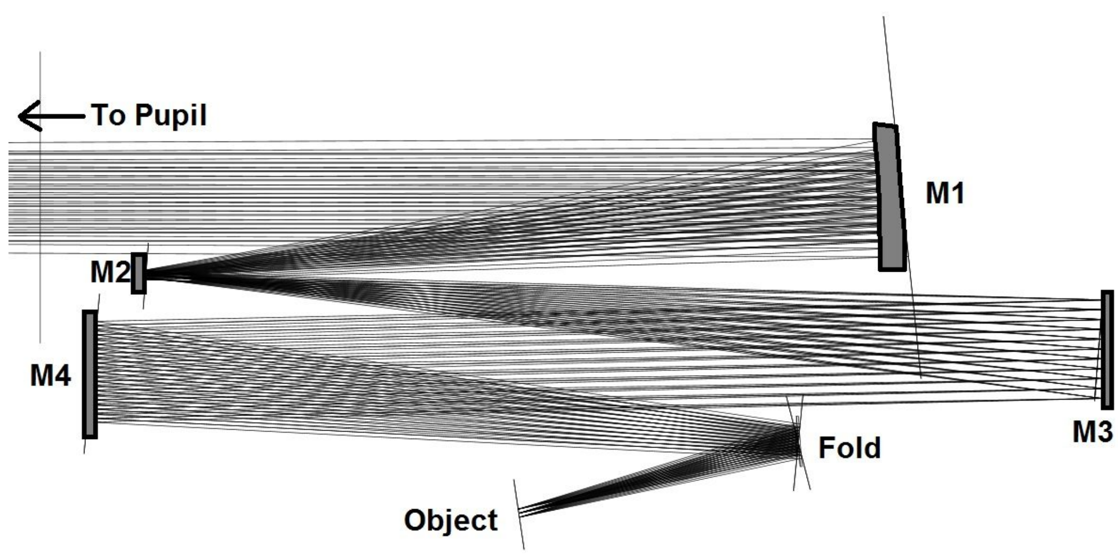

Figure 4: System Ray Trace for Collimator. In this case, the fold mirror is shown.

The sizes and prescriptions of the main mirrors are shown in Table 1.

Table 1: Main Mirror Prescriptions.

Mirror ID#	Radius (mm)	Conic Const.	Offset (mm)	Shape	Size (mm)
M1	-1509.309	-0.4258	-180.75	Rectangular	160 x 400
M2	609.184	0	0	Rectangular	22 x 80
M3	-1757.363	-0.8088	-66.21	Circular	ϕ 125
M4	-2090.74	-2.996	45.77	Rectangular	134 x 190

Although the size of the output pupil is relatively modest with a diameter of 85 mm, its remoteness from the collimator optics increases the size of the individual mirrors. The first mirror, M1 is over 3 m from the exit pupil location and, taking into account the maximum field angle of 4.4° along the slit direction, the mirror has to be sufficiently large to accommodate all fields. Combination of mirror size, geometry and form error requirement (<15 nm RMS) make the manufacture of these components a challenging proposition. Furthermore, restriction of background light due to scattering from mirror surfaces requires that the surface roughness of the mirrors must be closely controlled. In view of this, a surface roughness of less than 1 nm is specified.

3: DESIGN PERFORMANCE

3.1 Imaging and Wavefront Error

Of prime concern as a performance metric is the wavefront error of the collimator system. Indeed, the system prescription was primarily optimised on the basis of form error over the entire field. As far as the intrinsic design is concerned, the RMS wavefront error averaged over all fields is about 13 nm RMS. Of course, this is substantially less than the requirement of 30 nm RMS. However, due to the complex nature of the optical surfaces concerned, adequate allowance needs to be made for manufacturing shape errors.

Since the design, by deliberate choice, is 'slow', wavefront errors are dominated by low spatial frequency contributions. In particular, field curvature and astigmatism dominate, with some contribution from spherical aberration and coma. With regard to field curvature, due to the off-axis design, the focal plane is not perpendicular to the chief ray, but slightly inclined. Figure 5 shows a plot of rms wavefront error versus field angle along the 4.4° slit direction.

The wavefront error performance is clearly satisfactory. In addition, the telecentricity of the design across the entire field is better than 6 arcminutes and the image distortion is less than 0.15%.

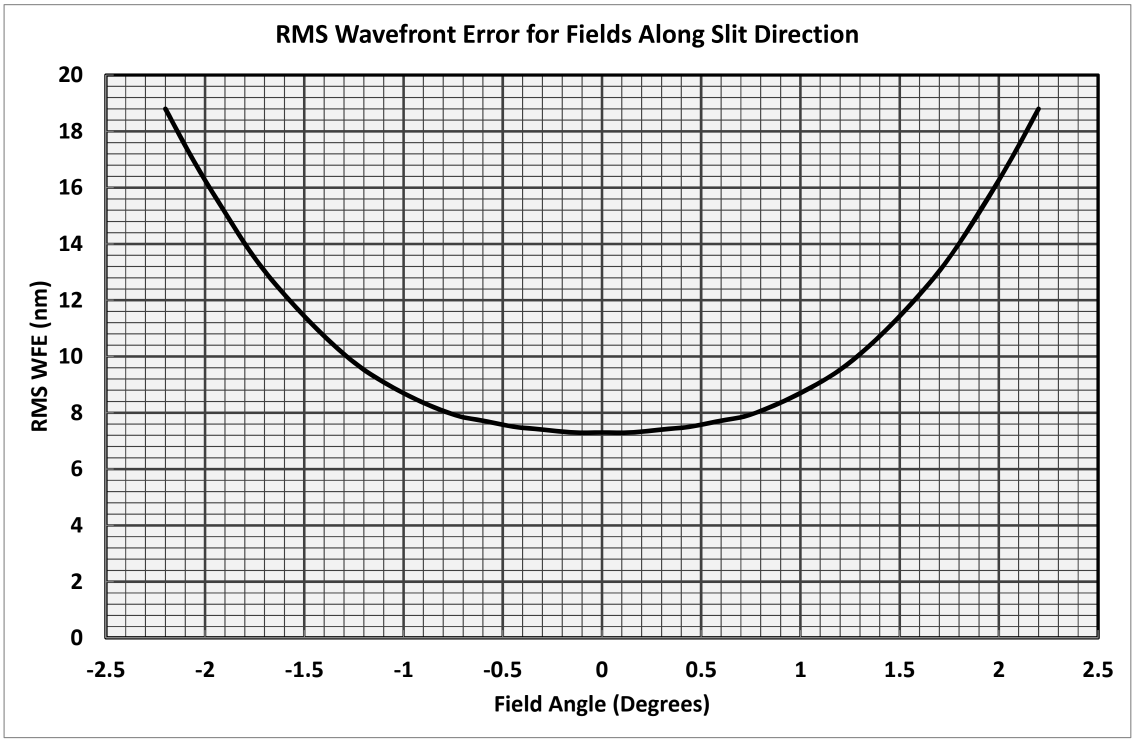

Figure 5: Wavefront error versus field angle along slit direction. Wavefront error variation across the slit direction is much smaller on account of the narrower field.

3.2 Alignment and Tolerancing

The most critical aspect relating to the tolerancing of the design is the form errors introduced into the manufacturing process. In addition, of course, alignment errors during system assembly might be expected to add to any wavefront error. As part of the tolerancing process, however, a detailed table of mirror alignment sensitivities has been compiled. The justification for this is that detailed knowledge of the sensitivity of individual Zernike wavefront error components to specific mirror tilts and decentres enables alignment adjustment to, in part, compensate for some manufacturing errors. Use of this alignment compensation procedure formed part of the computer tolerance modelling methodology. Table 2 sets out the alignment adjustments available in the mechanical design of the collimator mounts.

Table 2: Available alignment adjustments for collimator mirrors. Axes are defined as follows: x axis is across the slit direction and the y axis is parallel to the slit. The z axis follows the direction of light propagation. θx represents a rotation about the x axis and so on.

Mirror	dx	dy	dz	θx	θy	θz
M1	± 2 mm	± 2 mm	± 4 mm	± 0.5°	± 0.5°	± 1.0°
M2	None	None	None	± 0.9°	± 0.9°	None
M3	None	None	None	± 0.9°	± 0.9°	None
M4	± 3 mm	± 3 mm	± 4 mm	± 0.9°	± 0.9°	± 1.0°

As outlined, the tolerance modelling included component alignment errors and compensation, as well as component form errors introduced by the manufacturing process. It is worth examining the modelling of shape error in a little more detail. Form errors introduced in the manufacturing process will be heavily skewed toward the lower spatial frequency domain. In many cases, simple tolerance modelling of form error does not take account of this salient point. Following the methodology adopted in previous studies[4,5], random shape errors were ascribed to each mirror based on Zernike polynomials. To take account of the spatial frequency variation, the magnitude of each Zernike term was weighted according to the inverse square of its radial order.

Tolerance analysis has been carried out to define the manufacturing tolerances, the necessary compensators to achieve the final wavefront error, the degrees of freedom and the range of adjustments. Tolerances have been defined based on the results of the tolerance analysis, including sensitivity analysis and Monte Carlo simulations. Tolerance on the conic constants is less than 0.1% of the value, ± 0.5 mm for the off-axis distance, ± 0.5 mm for the mirror dimensions and ± 1 mm for thickness. Tolerances on the radii of curvature are: ± 0.75 mm for M1, ± 0.6 mm for M2, ± 0.9 mm for M3 and ± 1.0 mm for M4. The shape error defined for each mirror is better than 18 nm rms within any 85 mm subaperture over the clear aperture for M1. For the spherical M2, located close to an intermediate image plane, the form error tolerance, at 30 nm rms, is more relaxed. For M3, the form error tolerance is 15 nm rms over the whole clear aperture, as is the tolerance for the fold mirror (M5). For M4, the tolerance is less than 15 nm rms within any 90 mm subaperture over the clear aperture for M4.

A wavefront error better than 27.95 nm rms is achieved for 90% of the Monte Carlo simulations, with a mean value of 23.20 nm rms. The defined compensators correspond to the degrees of freedom shown in Table 2. Adjustments in defocus (dz) are only required for the input and output beams (M1 and M4). The range of adjustments have been defined to satisfy the specification of the wavefront error regarding the minimum and maximum changes for each compensator obtained from the tolerances analysis and considering the constraints imposed by the available space. The ranges of adjustment for each degree of freedom are: ± 2 mm for dx and dy of M1, with a resolution of 0.0100mm, ± 0.5˚ for Θ_x and Θ_y for M1 with a resolution of 0.0057˚ and ± 4 mm for dz with a resolution of 0.0100 mm. For M2: ± 0.9˚ for Θ_x with a resolution of 0.0020˚ and ± 0.9˚ for Θ_y with a resolution of 0.0067˚. For M3: ± 0.9˚ for Θ_x with a resolution of 0.0016˚ and ± 0.9˚ for Θ_y with a resolution of 0.0015˚. For M4: ± 3mm for dx and dy with a resolution of 0.0100 mm, ± 0.9˚ for Θ_x with a resolution of 0.0012˚, ± 0.9˚ for Θ_y with a resolution of 0.0014˚ and ± 4 mm for dz with a resolution of 0.0100 mm. For the fold mirror (M5): ± 0.9˚ for Θ_x and Θ_y with a resolution of 0.0017˚ and 0.0037˚, respectively. The different resolutions presented for the same range of adjustment in each mirror vary as a function of the mirror aspect ratio and size, in combination with design constraints on the moment arm lengths of a flexure-type tip-tilt mount and adjustment screw thread pitch.

A surface roughness less than 1 nm rms in spatial frequency range between 1 μm and 0.1 mm is required for all mirrors and the surface defects specification is < 5/3 x 0.1 according to DIN ISO 10110-7.

3.3 Stray light Modelling

A detailed non-sequential, stray light model was built incorporating all optical surfaces, mounts and enclosure surfaces. The collimator system is preceded by an integrating sphere, four lenses (condensing optics) and the object target masks (Figure 2). The NSC optical design is presented in Figure 6 with (right) and without (left) the condensing optics.

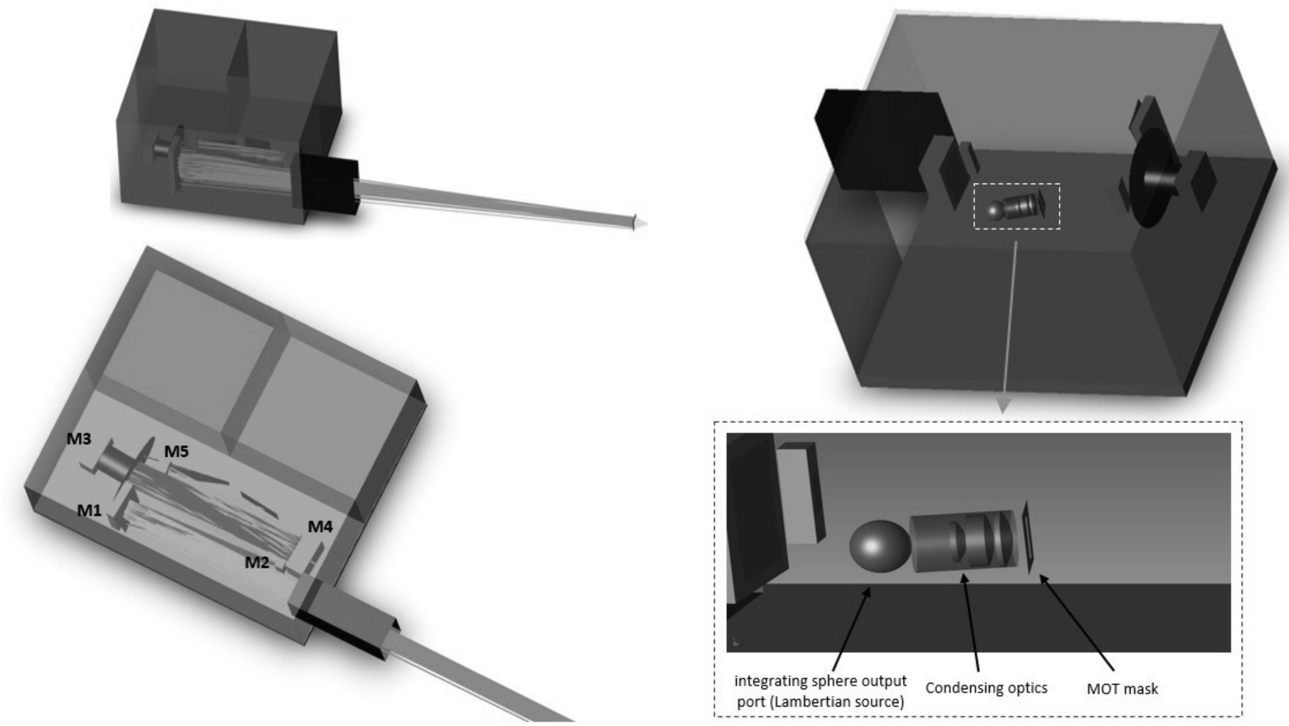

Figure 6: Non-sequential model of the Collimator system. On the left, two views of the four powered mirrors and the fold mirror (M5), with the breadboard, baffles, mounts and enclosure are shown. A paraxial lens has been added in the output collimated beam to evaluate the results at the instrument focal plane. On the right, the NSC design is shown including the integrating sphere, condensing optics and the moveable target mask.

Scattered contributions associated with surface roughness and particulate contamination, such as dust deposited on the mirror surfaces, were studied independently. In practice, the impact of scattering from the reflective mirrors dominates the stray light performance. For this reason, the surface roughness of the mirrors must be adequately controlled and a maximum roughness of 1 nm rms has been set out. As in the case of form error, surface roughness contributions decline as a function of spatial frequency. It is expected that the relevant power density spectrum (PSD) shows a power density that can be modelled by an inverse square dependence upon spatial frequency, not unlike the form error. Since the surface roughness is very small compared to the wavelength, the total integrated scattered may be accounted for by the 'small signal approximation'.

$$S = \left(\frac{4\pi\sigma_{rms}}{\lambda} \right)^2 \tag{1}$$

S is the proportion of light scattered; σ_{rms} is the surface roughness; λ is the wavelength.

For example, at the shortest UV wavelength of interest, 305 nm, the total integrated scattering is 0.17%. The PSD spectrum impacts the angular distribution of the scattered light with low spatial frequency surface roughness equating to small angle scattering. This results in the so called ABC or K-Correlation model for scattering where the BSDF (Bi-directional scattering distribution function) is described by the following equation:

$$BSDF = \frac{A\beta}{\left(1 + B^2\beta^2/\lambda^2\right)^{(c+1)/2}} \tag{2}$$

where: β is the cosine of the scattered angle and A, B and C are constants.

To evaluate the contribution of surface roughness, the mirrors have been modelled according to ABC scatter model (K-Correlation scatter model)[7], with the following parameters: an effective surface roughness of 1 nm rms; the shortest wavelength of the spectral range has been considered as the reference wavelength, 0.305 µm; a log-log slope of the Bi-directional Scattering Distribution Function at large spatial frequencies of S=3 and a B parameter B ≈ 104 µm. All non-optical surfaces were modelled as surfaces with a Lambertian scattering of 3%, defined as mirrors with a coating of 3% reflectivity and a scattered fraction of 1. The stray light analysis was performed for the various moveable object targets (MOT) of Figure 2. They can be listed according to their associated stray light contribution in decreasing order as follows: sharp edge, slit, broadband partial slit, pinhole for focussing tool and monochromatic partial slit.

Another contribution to the stray light is related to surface cleanliness. Dust deposited on the mirrors surfaces gives rise to scattering. In this analysis, we use a conservative assumption of a surface with a surface cleanliness level of 200, as defined[8] in MIL-STD-1246. The K-correlation scatter model[7] was applied, modifying the parameters previously defined for the surface roughness according to the approach adopted by Peterson et al.[9]. The slope parameter is now S=0.926 and an effective roughness (sigma) of 0.24 nm has been calculated for a total integrated scattering per surface of $1 \cdot 10^{-4}$. After performing both analyses individually, it can be concluded that the dust contribution is not significant compared to that due to surface micro-roughness.

The source has been modelled as a circular, Lambertian emitter with a diameter of 10 mm, as per the integrating sphere output port. The condensing optics have been integrated to the model within a barrel including a mount per lens and a mask has been defined for each moveable object target. The MOT mask is separated from the lenses barrel 10 mm in order to replicate a realistic scenario that considers the mechanism to select the mask of interest. Due to this separation, some additional background scattering contribution will be added to the target signal. In order to quantify this contribution, an opaque mask has been defined at the target position with the same size as the relevant object (MOT). The environmental contribution is very low, with an average value of 1.53E-09 Watts/cm^2. The ratio of the environmental contribution with respect to the sharp edge average value is 1.29E-04, so the background level is four orders of magnitude lower than the contribution associated to the sharp edge.

The illumination uniformity was evaluated by placing a detector with the sharp edge aperture size at the target position. The specification establishes that the intensity variation of the sharp edge illumination should be smaller than ± 10% in x direction and smaller than ± 20% in y direction. The values for every pixel of the detector were analysed. The average for each row was calculated and those values were normalised to the maximum. The illumination along a column varies between a minimum value of 0.923 and a maximum of 1.05, and, across the column, the difference in illumination is 3.1E-04, and within the specification.

The level of background stray light that would be attributable to diffraction was evaluated in the preliminary design of the collimator system and it was found to be negligible. In the final design, we need to assess the localised PSF contribution of diffraction in the region close to the edge of a feature. More specifically, this was done by modelling the diffraction pattern around the edge of an incoherently illuminated sharp edge. As a worst case scenario, the analysis was pursued for a wavelength of 775nm. We replicate the convolution of an Airy pattern attributable to a f#10 aperture around the edge of the sharp edge. This is shown in Figure 7, which plots the irradiance against the angle in arcminutes and compares the relative irradiance with the effect of scattering. It is clear that the effect of diffraction is negligible when compared to scattering. If the original scattering profile were convolved with the diffraction pattern there would be very little change. This is not surprising, as the effective 'Rayleigh Criterion' angle associated with a f#10 aperture at 775 nm is about 0.04 arcminutes.

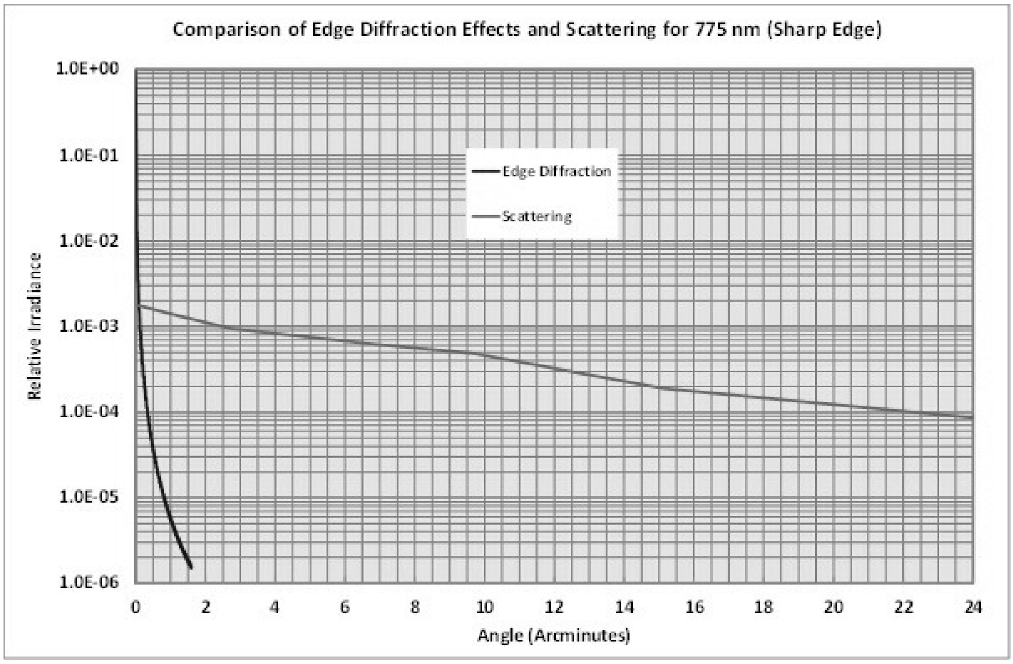

Figure 7: Comparison of Edge Diffraction and Scattering Effects at 775 nm.

3.4. Mechanical Aspects

Thermal distortion of the collimator system was modelled for a temperature variation of ±2°C. The very small alignment changes produced had a negligible effect on the system wavefront error. This investigation was repeated for mechanical distortions produced by routine mechanical movement of the object target assembly. Again, this has a negligible impact upon the system performance. All mirrors are to be mounted in a specially designed flexure mount where the flexure of compliant invar pads allows for relative thermal expansion of the mirrors without producing stress induced deformation. The modelled deformation is shown in figure 8.

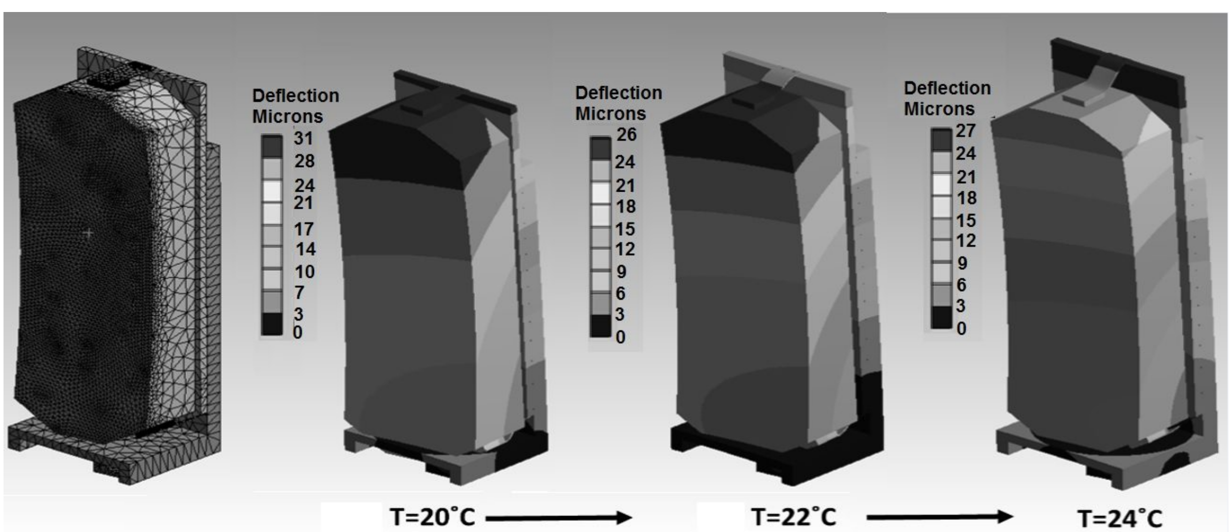

Figure 8. Finite element analysis of Mirror 1 showing the deflection due to thermal loading

4 CONCLUSIONS

A high fidelity collimation system has been developed for use in the calibration of a satellite based imaging spectrometer. The design is loosely based on a three mirror anastigmat design with a fourth mirror introduced to ensure a telecentric input. Performance of the system has been extensively modelled and the system conforms to the image quality and straylight requirements set out.

5 ACKNOWLEDGEMENTS

The authors acknowledge the European Union, the European Space Agency, EUMETSAT, Airbus DS and Mullard Space Science Laboratory. This document has been produced with the financial assistance of the European Union. The views expressed herein can in no way be taken to reflect the official opinion of the European Union and/or ESA. The authors would also like particularly to thank J.F. Pittet of Airbus DS for many useful discussions.

6 REFERENCES

[1] Bazalgette Courrèges-Lacoste, G., Ahlers, B., Guldimann, B., Short, A., Veihelmann, B. and Stark, H., "The Sentinel4/UVN instrument on-board MTG-S", Proc. EUMETSAT Meteorological Satellite Conf., 5–9 September 2011, Oslo, Norway, p. 59 (2011)

[2] Noëll, S., Bramstedt, K., Bovensmann, H., Gerilowski, K., Burrows, J. P., Standfuss, C., Dufour, E. and Veihelmann, B., "Quantification and mitigation of the impact of scene inhomogeneity on Sentinel-4 UVN UV-VIS retrievals", Atmos. Meas. Tech., **5**, 1319–1331, (2012)

[3] Korsch D., "Closed form Solution for three-mirror telescopes, corrected for spherical aberration, coma, astigmatism, and field curvature", Appl. Opt. **11**, 2986 (1972)

[4] Lampton, M., Sholl, M., "Comparison of on-axis three-mirror-anastigmat telescopes", Proc. SPIE **6687**, 66870S (2007)

[5] Rolt, S, Dubbeldam, C. Marc, Robertson, David J., Ryder, David A., "Design for test and manufacture of complex multi-component optical instruments", Proc. SPIE **7102**, 71020A (2008)

[6] Rolt, S., "A review of the KMOS IFU component metrology programme", Proc. SPIE **8450**, 84500O (2012)

[7] Dittman, M. G., "K-correlation power spectral density & surface scatter model", Proc. SPIE 6291, Optical Systems Degradation, Contamination, and Stray Light: Effects, Measurements, and Control II, 62910R (2006).

[8] MIL-STD-1246, "Military standard product cleanliness and contamination control program", US Department of Defense, (1991)

[9]: Peterson, R. V., Magallanes, P. G., Rock, D. F., "Tailored Particle Distributions Derived from MIL-STD-1246". Proc. SPIE, Vol. 4774: Optical System Contamination: Effects, Measurements, and Control VII (2002).